


## Calixarene-Based lead receptors: an NMR, DFT and X-Ray synergetic approach

Ana S. D. Ferreira , José R. Ascenso , Paula M. Marcos , Rachel Schurhammer , Neal Hickey and Silvano Geremia 

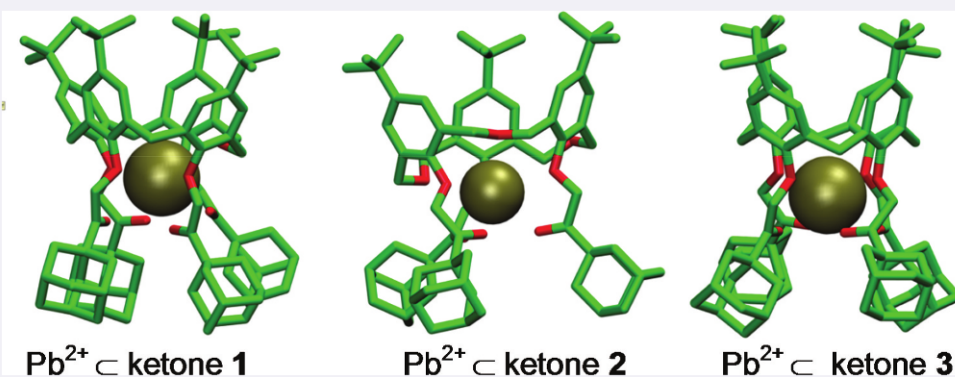
<sup>a</sup>UCIBIO, Departamento de Química da Faculdade de Ciências e Tecnologia, Universidade Nova de Lisboa, Caparica, Portugal; <sup>b</sup>Instituto Superior Técnico, Centro de Química Estrutural, Lisboa, Portugal; <sup>c</sup>Centro de Química Estrutural, Faculdade de Ciências da Universidade de Lisboa, Lisboa, Portugal; <sup>d</sup>Departamento de Ciências Farmacêuticas e do Medicamento, Faculdade de Farmácia da Universidade de Lisboa, Lisboa, Portugal; <sup>e</sup>Université de Strasbourg, Laboratoire de Modélisation Et Simulations Moléculaires, Strasbourg, France; <sup>f</sup>Centre of Excellence in Biocrystallography, Department of Chemical and Pharmaceutical Sciences, University of Trieste, Trieste, Italy

### ABSTRACT

The conformational changes of the homooxa adamantyl ketones **1** and **2**, as well as of the calix[4]arene analogue derivative **3**, all in the cone conformation, upon  $\text{Pb}^{2+}$  complexation were investigated by  $^1\text{H}$ ,  $^{13}\text{C}$ ,  $^{207}\text{Pb}$  NMR and proton spin-lattice relaxation times ( $T_1$ ) experiments. The X-ray crystal structures of ketones **1** and **3** were determined. The inclusion of an acetonitrile molecule in the hydrophobic cavity of the ligands was observed in the solid state. In solution, inclusion was observed only in the case of  $\text{Pb}^{2+}$   $\subset$  ketone **3** complex. DFT calculations were also performed to complement the NMR conformational analysis and to bring further insights to the cation complexation. The data confirmed the formation of 1:1 complexes between  $\text{Pb}^{2+}$  and the ligands, and that the cation is located inside the cavity defined by the phenoxy and carbonyl oxygen atoms. In general, the ligand conformations became closer to a regular cone upon complexation, with the binding models found for the three ketones through the NMR studies corroborated by the DFT calculations.

### KEYWORDS

Calixarene adamantyl ketones;  $\text{Pb}^{2+}$  binding; NMR studies; DFT calculations; X-ray diffraction



### Introduction

Lately, increasing attention has been paid to the coordination chemistry of heavy metals, such as arsenic, cadmium, mercury and lead. These metals, resulting from industrial processes, are very toxic and difficult to remove, thus provoking a harmful impact on environmental quality and consequently on human health [1,2]. In fact, from soil and water contamination, these heavy metals enter into the food chain and can induce serious problems in human health.  $\text{Pb}(\text{II})$  is one of the heavy metal ions broadly present in the environment. Even at

very low concentrations, lead can cause severe damages in the human brain and nervous system, increasing the risk of neurodegenerative diseases, as well as kidney, bone and cardiovascular pathologies [3].

Calixarenes are a versatile family of macrocyclic compounds widely investigated in host-guest and supramolecular chemistry [4,5]. Their availability and relatively easy functionalization at the upper and lower rims afford a large variety of derivatives, with multiple possibilities of applications in different areas, such as extraction, sensing and recognition of

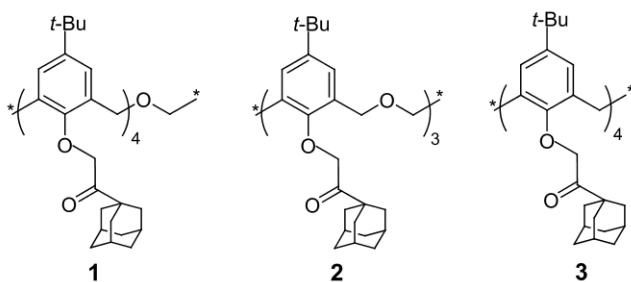


**Figure 1.** Chemical structures of adamantyl ketones **1**, **2** and **3**.

relevant ions and neutral molecules [6–8]. In particular, lower rim functionalised calixarenes with carbonyl groups have shown a strong ability towards different metal cations [9,10]. Among them, certain calixarene derivatives have been recognised as useful ionophores for  $\text{Pb}^{2+}$  ion. The carbonyl and the phenoxy oxygen atoms play an important role in  $\text{Pb}^{2+}$  binding. Very recent articles report studies with calix[4]arene tetraacetic acid [11] and amide derivatives [12–14] in solvent extraction systems and electrochemical sensors for  $\text{Pb}^{2+}$  determination.

In the course of our systematic research on the binding properties of homooxacalixarenes [15] bearing ketonic carbonyl groups at the lower rim [16–21], we were interested in determine how the cation complexation would influence the calixarene conformation. Thus, the conformational analysis of the homooxa adamantyl ketones **1** and **2**, and their conformational changes upon  $\text{Pb}^{2+}$  complexation, were assessed by  $^1\text{H}$ ,  $^{13}\text{C}$ ,  $^{207}\text{Pb}$ , 2D NMR experiments and proton spin-lattice relaxation times ( $T_1$ ). The X-ray crystal structures of ketones **1** and **3** were determined, and DFT computational studies were performed to add further insights to the binding process. Tetraadamantyl ketone derivative **3** of the *p*-*tert*-butylcalix[4]arene (Figure 1) was also studied in this work, and the results of the three ligands were compared and discussed in order to analyse the effects of the additional oxygen bridges on the macrocycle conformational flexibility.

## Materials and methods

### Materials

Adamantyl ketones **1**, **2** and **3** were synthesised according to the procedures reported in the literature (20, 18 and 21, respectively). Lead (II) perchlorate hydrate 98% was purchased from Sigma-Aldrich and it was dried over  $\text{P}_4\text{O}_{10}$  under vacuum for several days before use.

### Determination of the crystallographic structures of **1** and **3**

Single crystals suitable for X-ray diffraction structure analysis were obtained by slow evaporation of solutions of the adamantyl ketones **1** or **3** in various mixtures of organic solvents. The crystallisation trials in the presence of lead acetate did not yield any structure with encapsulated  $\text{Pb}^{2+}$ . Two pseudo-polymorphic forms for both adamantyl ketones **1** and **3** were obtained in the presence or absence of the co-solvent acetonitrile, which exhibits guest properties towards the calixarene cavity. Data collection was carried out at the Macromolecular crystallography XRD1 beamline of the Elettra synchrotron (Trieste, Italy), employing the rotating-crystal method with a Dectris Pilatus 2 M area detector. Single crystals were dipped in paratone cryoprotectant, mounted on a nylon loop and flash-frozen under a nitrogen stream at a 100 K. Diffraction data were indexed and integrated using the XDS package [22], while scaling was carried out with XSCALE [23]. Structures were solved using the SHELXT program [24] and structure refinement was performed with SHELXL-18/3 [25], operating through the WinGX GUI [26], by full-matrix least-squares (FMLS) methods on  $F^2$ . Non-hydrogen atoms were refined anisotropically, with the exception of some disordered groups. Hydrogen atoms were added at the calculated positions and refined using the riding model. Crystallographic data are reported in Table S1. Full detailed refinement procedures are reported in the Supporting Information (Figure S1).

### NMR studies

The NMR experiments were performed in  $\text{CDCl}_3$  at  $25^\circ\text{C}$  using a Bruker Avance III 500 spectrometer. TMS was used as internal reference for  $^1\text{H}$  and  $^{13}\text{C}$  NMR measurements, while for  $^{207}\text{Pb}$  chemical shifts a 1.0 M solution of  $\text{Pb}(\text{NO}_3)_2$  in  $\text{D}_2\text{O}$  was used as external calibration ( $\delta = -2961.2$  ppm relative to  $\text{Pb}(\text{CH}_3)_4$ ). The  $^{207}\text{Pb}$  spectra were acquired using a  $90^\circ$  pulse of  $10.2 \mu\text{s}$  and a relaxation delay time of 0.6 s. The NOESY and HMBC 2D NMR spectra were acquired using the Bruker standard pulse sequences. The NOESY experiments were collected as a 256x2K complex points and a mixing time of 0.6 s and the HMBC as 512x1K data points and a relaxation delay time of 1.5 s. Spin-lattice relaxation times ( $T_1$ ) were determined by the inversion recovery method [27], in which 16 spectra of 32 K data points were collected, with 16 inversion recovery delay times ( $\tau$ ) ranging from 50 ms to 2 s. A quick  $T_1$  estimation was performed for all samples to set the appropriate

relaxation delay between 2 and 5 s. The  $T_1$  values were obtained by fitting the data to the equation:

$$1/4 I_1 \left( 1 - 2e^{-\frac{t}{\tau}} \right)$$

where  $I$  is the magnetisation,  $I_\infty$  is the magnetisation at thermal equilibrium and  $\tau$  is the inversion time.

The complexation studies were carried out by adding 1 equiv of the salt  $\text{Pb}(\text{ClO}_4)_2$  (0.25 M) in  $\text{CD}_3\text{OD}$  to 0.5 mL of  $\text{CDCl}_3$  solutions ( $5 \times 10^{-3}$  M) of the ligands directly in the NMR tube, the  $^1\text{H}$  and  $^{13}\text{C}$  spectra being recorded after the addition. For the titrations with MeCN, several aliquots (up to 10 equiv) of MeCN solution in  $\text{CDCl}_3$  ( $1.25 \times 10^{-1}$  M) were added to the free ligands and to the  $\text{Pb}^{2+}$  c ketone complexes. In the case of the  $^{207}\text{Pb}$  spectra, the experiments were performed by adding 1 equiv of the ligands to a  $\text{CDCl}_3/\text{CD}_3\text{OD}$  (10:1) solution of the salt ( $5 \times 10^{-2}$  M) directly in the NMR tube.

### DFT calculations

Stationary points were optimised with the Gaussian 09 program [28] with different functionals for comparison: B3LYP [29], BP86 [30], M06-2X [31] and wB97XD [32] functions with the 6-31 G(d,p) basis for C, N, O, H atoms and SDD for lead. A D3-Grimme correction [33] was also used associated to B3LYP and BP86 functionals. Experimental X-ray diffraction structure determination results were employed as the starting structures for geometry optimisation. All reported structures were confirmed as energy minima, with no negative eigenvalue in the Hessian matrix. The  $^{13}\text{C}$  NMR calculations employed the Gauge-Independent Atomic Orbital (GIAO) method [34]. An average of values of equivalent atoms was assumed.

## Results and discussion

### X-Ray diffraction studies

The X-ray structures of two pseudo-polymorphic forms ( $\alpha$  and  $\beta$ ) for adamantyl ketones **1** and **3** were determined using synchrotron radiation with cryogenic techniques.

The dihomooxalix[4]arene macrocycle **1** shows the expected cone conformation in both crystal forms (Figure 2a,b). The planes of the phenyl rings A and B (connected to the dihomooxa bridge) of **1 $\alpha$**  make dihedral angles of  $120.6^\circ$  and  $62.6^\circ$  with respect to the mean plane of the methylene bridging groups (Table 1). Angles greater than  $90^\circ$  indicate that the *tert*-butyl groups on the upper rims lean outwards from the centre of the cone (Figure 2a) and vice versa. Therefore, the A and B are oriented outwards and inwards, respectively.

**Table 1.** Comparison of cone conformations: dihedral angles between corresponding aryl planes of the calixarene cones (A, B, C and D) and the mean planes of the bridging methylene carbon atoms and torsion angles (between parentheses) around the O-CH<sub>2</sub> bond determining the orientation of the carbonyl and adamantyl groups. See Figure 2a for the labelling scheme of the arene moieties.

|                             | A             | B             | C             | D             |
|-----------------------------|---------------|---------------|---------------|---------------|
| <b>1<math>\alpha</math></b> | 120.6 (−81.5) | 62.6 (−160.9) | 148.1 (−58.3) | 104.3 (167.7) |
| <b>1<math>\beta</math></b>  | 102.0 (180.0) | 141.9 (−56.6) | 96.5 (168.4)  | 132.9 (−57.2) |
| <b>3<math>\alpha</math></b> | 135.3 (50.5)  | 94.6 (−167.9) | 135.3 (50.5)  | 94.6 (−167.9) |
| <b>3<math>\beta</math></b>  | 112.1 (124.8) | 117.9 (120.6) | 111.5 (129.1) | 114.6 (121.8) |

The planes of the phenyl ring C makes a dihedral angle of  $148.1^\circ$  with the mean plane of the methylene bridging groups, with the upper rim largely inclined outwards, while the phenyl ring D is tilted slightly outwards, with a dihedral angle of  $104.3^\circ$ . This distorted cone conformation, with one inward oriented phenyl ring involved in the dihomooxa bridge, appears to be a characteristic feature of dihomooxalix[4]arenes functionalised with *tert*-butyl groups on the upper rim and four substituents on the lower rim, in absence of a guest [35–37]. In the presence of a guest molecule, the macrocycle necessarily opens its cup to host the molecule, thereby altering its conformation, as observed in the **1 $\beta$**  form which hosts an acetonitrile molecule in the cup. In this case, the dihedral angles of phenyl rings are all oriented outwards (Table 1 and Figure 2b). The orientation of the phenyl groups is reflected in the position of the adamantyl substituents on the lower rim. In the  $\alpha$  form, the adamantyl group of the most outwardly oriented C ring is more internal and aligned with the central axis of the molecule, while the adamantyl group of the inwardly oriented B ring protrudes more than the others (Figure 2a). Consistently, in the  $\beta$  form with all the phenyl rings outwardly oriented, the adamantyl groups are more closely packed (Figure 2b). The orientation of the adamantyl and carbonyl groups are mainly dictated by the torsion angle around the O-CH<sub>2</sub> bond (Table 1). In both crystal forms two carbonyl groups are internally oriented but on different rings (B, D for **1 $\alpha$**  and A, C for **1 $\beta$** , see Table 1 torsion angles close to  $180^\circ$ ). The layer organisation of the crystal packing of **1 $\alpha$**  (Figure 3a) produces two types of solvent channels along the crystallographic a axis, which contain the disordered co-crystallised solvent molecules (Figure 4a). On the contrary, the more closed packed  $\beta$  form shows interrupted channels along the crystallographic b axis, therefore producing enclosed cavities occupied by the solvent molecules (Figure 4b).

The calix[4]arene macrocycle **3** shows the expected cone conformation in both pseudo-polymorphic forms (Figure 2c,d). In the  $\alpha$  form the molecule shows a  $C_2$

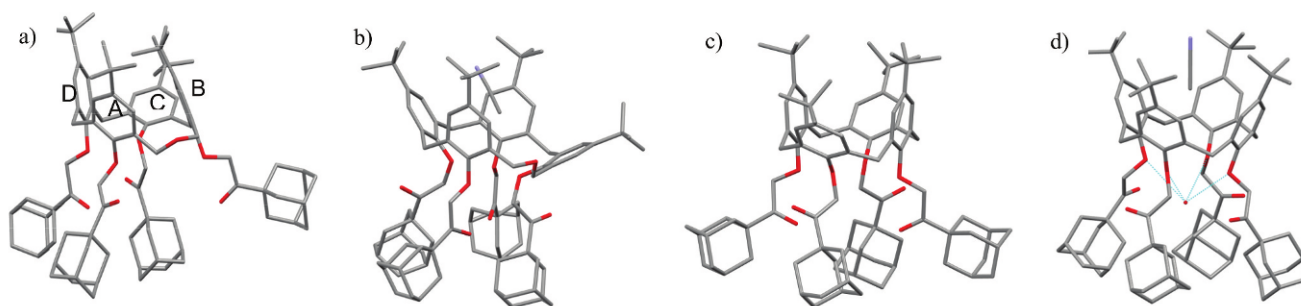


**Figure 2.** Stick representation of X-ray structures of a) **1α**, b) **1β**, c) **3α** and d) **3β**. The atomic species are represented in CPK colours. Hydrogen atoms are omitted for clarity.

symmetry with two opposite phenyl rings more outwardly inclined ( $135.3^\circ$ ) with the other two nearly orthogonal ( $94.6^\circ$ ) with respect to the mean plane of the methylene bridging groups. In the  $\beta$  form, in which the molecule hosts an acetonitrile guest molecule, a pseudo  $C_4$  symmetry is observed with the planes of the phenyl rings making similar dihedral angles, ranging from  $111.5^\circ$  to  $117.9^\circ$  (Table 1). This acetonitrile guest forms the typical host-guest CH- $\pi$  interactions. The **3β** structure shows a water molecule entrapped on the lower rim by H-bond with the phenoxy oxygen atoms (Figure 2d). This assignment is supported by the high resolution electron density maps (Figure S1f). A water molecule entrapped between the oxygen on the lower rim has been previously reported for analogous calix[4]arene [38]. Similarly to both **1** structures, in **3α** two opposite carbonyl groups are oriented inwards (Table 1). On the contrary, in **3β** the carbonyl groups are oriented orthogonally with respect to the symmetry axis of the molecule in a way to maintain the pseudo  $C_4$  symmetry. This produces a dissymmetric conformation of the calix[4]arene, with the orientation of the carbonyl and adamantyl groups dictated by the torsion angle around the O-CH<sub>2</sub> bond ranging from  $120.6^\circ$  to  $129.1^\circ$  (Table 1). The position of the entrapped water molecule is reminiscent of the coordination of Pb<sup>2+</sup> ions found in analogues calix[4]arene functionalised on the lower rim with four ketone groups, four ester groups [39] or four amide groups [40]. In these structures the lead shows eightfold oxygen coordination. In the case of the ketone and ester groups, which are more closely related to **3**, the oxygen atoms are arranged as the corners of a tetragonally compressed cube [39], while they are arranged in an intermediate shape between a cube and a square antiprism for the amide derivative [40]. Comparison of the intramolecular assembly of the adamantyl groups shows that the calix[4]arene complexed by the guest molecules is more compact than the free calix[4]arene (Figure 2c,d). In the  $\alpha$  structure the  $C_2$  symmetric pinched cone

conformation forces two opposite adamantyl groups outwards from the symmetry axis (Figure 2c). The crystal packing of **3α** is characterised by a 1D stacks of calix[4]arene molecules (Figure 3c). This results in a very open structure with an interconnected network of solvent accessible channels (Figure 4c). In the case of **3β**, the head-to-head/tail-to-tail organisation of the crystal packing (Figure 3d) produces cavities, which contain the disordered co-crystallised solvent molecules (Figure 4d).

## NMR and DFT conformational analysis

### Proton and carbon-13 studies

The ionophoric properties of homooxalixarene ketone derivatives were previously reported [17,18], showing that these ligands form 1:1 complexes with heavy metal cations, such as Pb<sup>2+</sup>. Limitations in the solubility of adamantyl ketone derivatives prevented however the determination of their stability constants. The <sup>1</sup>H NMR data indicated that the cations were encapsulated inside the cavity formed by the phenoxy and carbonyl oxygen atoms. Following this line of research and to gain further information on the cation binding behaviour of the ligands, namely concerning the binding sites, homooxalixarene ketones **1** and **2**, as well as calix[4]arene ketone **3** were studied through <sup>1</sup>H, <sup>13</sup>C, <sup>207</sup>Pb and  $T_1$  relaxation NMR experiments.

Proton NMR data of the free and complexed ligands **1**, **2** and **3** were obtained and are in agreement with the results previously reported [17,18,41]. Similarly, <sup>13</sup>C NMR data were obtained. All the assignments were confirmed by DEPT, and by NOESY and HMBC 2D NMR experiments.

Concerning dihomooxalixarene ketone **1**, the conformational analysis in CDCl<sub>3</sub> indicated a molecule with a symmetry plane, with the following characteristic <sup>1</sup>H and <sup>13</sup>C signals of a cone conformation: two singlets for the *tert*-butyl protons, three AB quartets (in a 2:2:1 ratio) for the CH<sub>2</sub> bridge protons and two pairs of doublets for the aromatic protons of the calixarene framework (Figure 5a)

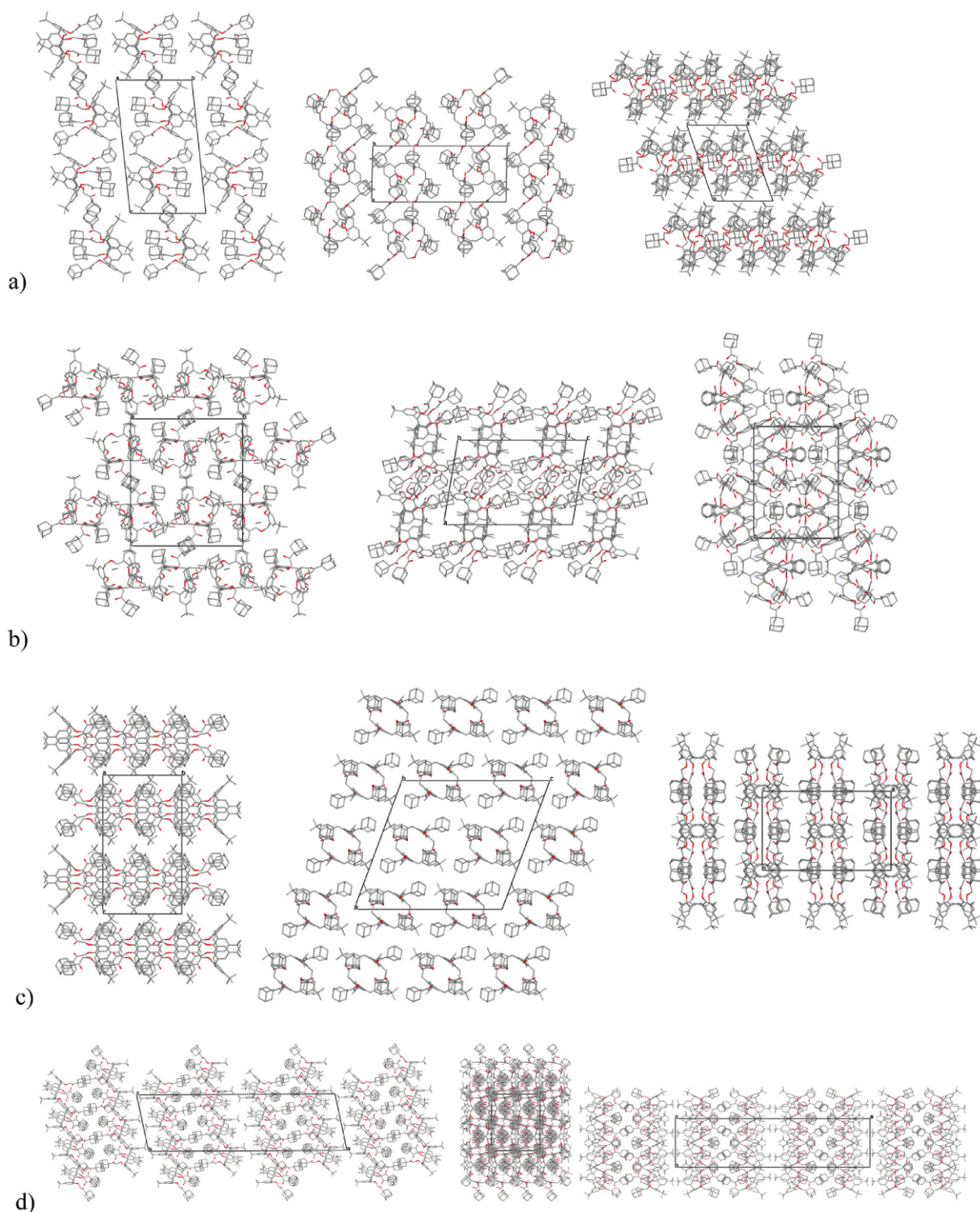


**Figure 3.** Crystal packing views along the a, b and c unit cell axes of the X-ray structures of a) **1a**, b) **1b**, c) **3a** and d) **3b**.

[42], as well as two ArCH<sub>2</sub>Ar resonances around 32 ppm [43]. Protons corresponding to rings A and B (Figure 5c) were identified by the NOESY experiments (Figure S2). Upon Pb<sup>2+</sup> complexation, all the proton (Figure 5b) and carbon-13 chemical shifts (Table S2) in ligand **1** are

affected. The highest upfield shift variations were observed for the bridging axial methylene protons (ArCH<sub>2</sub>Ar) and the oxygen bridge equatorial and axial methylene protons (CH<sub>2</sub>OCH<sub>2</sub>), while the largest downfield changes were observed for the aromatic protons,

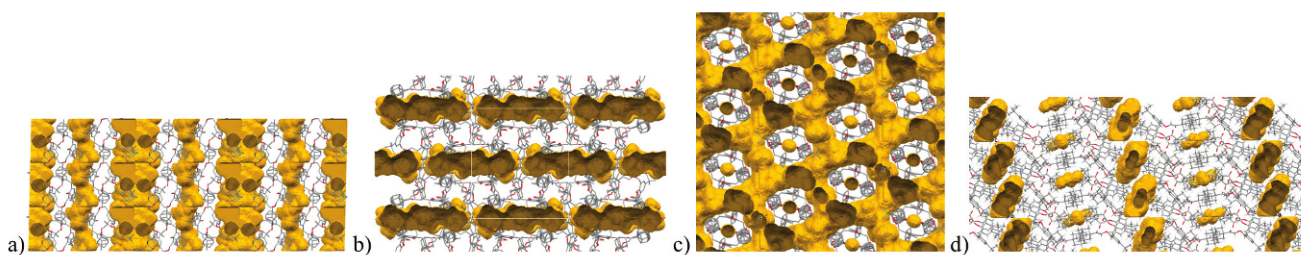


**Figure 4.** Accessible void volume of X-ray structures of a) **1a**, b) **1β**, c) **3a** and d) **3β**.

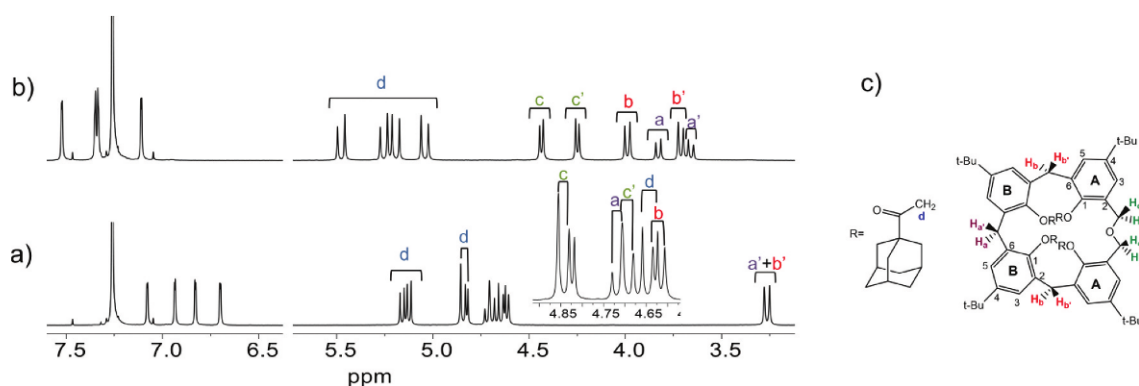


**Figure 5.** Partial <sup>1</sup>H NMR spectra (500 MHz, CDCl<sub>3</sub>, 25°C) of: a) Ad ketone **1**, insert: 4.5–4.9 ppm region expansion; b) **1** + 1 eq of Pb(ClO<sub>4</sub>)<sub>2</sub>; c) Rings and atoms identification in **1**.

the methylene protons of the OCH<sub>2</sub>CO groups and for the equatorial methylene protons of the ArCH<sub>2</sub>Ar bridges.

Gutsche ([4a]) established that the difference in the chemical shifts between the axial and the equatorial protons of the ArCH<sub>2</sub>Ar bridges indicates the degree of flattening of the cone conformation. A value around 0.9 ppm means a regular cone and zero a regular 1,3-alternate conformation. Upon Pb<sup>2+</sup>

complexation, the  $\Delta\delta_{\text{Hax-Heq}}$  decreases from 1.39 ppm to 0.22 ppm (in average), indicating that the pendant arms of ketone **1** move closer together, resulting in a more flattened cone conformation. In addition, both axial and equatorial methylene protons of CH<sub>2</sub>OCH<sub>2</sub> bridge move upfield and with the same value, suggesting significant conformational changes on the oxygen bridge upon complexation.

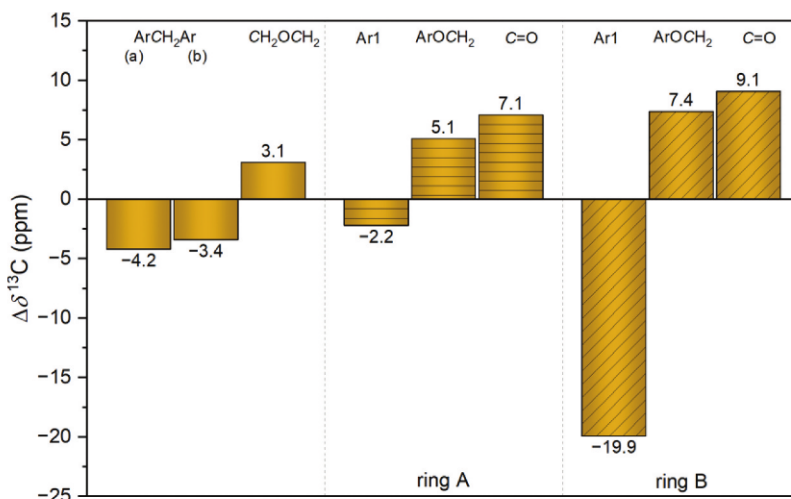


**Figure 6.** Largest <sup>13</sup>C chemical shift differences for ligand **1** upon Pb<sup>2+</sup> complexation [ $\delta(\text{Pb}^{2+} \cdot \mathbf{1}) - \delta(\mathbf{1})$ ].

Table 2.  $^{13}\text{C}$  NMR chemical shift variations\* for ligand **1** upon  $\text{Pb}^{2+}$  complexation obtained by NMR and DFT (M06-2X) calculations.

|     |          | Ketone <b>1</b> |      |                 |     |                                  |      |                      |       |      |                 |      |     |     |      |     |                 |      |     |      |                    |      |     |     |
|-----|----------|-----------------|------|-----------------|-----|----------------------------------|------|----------------------|-------|------|-----------------|------|-----|-----|------|-----|-----------------|------|-----|------|--------------------|------|-----|-----|
|     |          | Ad              |      |                 |     | CH <sub>2</sub> OCH <sub>2</sub> |      | ArCH <sub>2</sub> Ar |       |      | Aromatic ring A |      |     |     |      |     | Aromatic ring B |      |     |      |                    |      |     |     |
| C   | $\delta$ | CH <sub>3</sub> | CH   | CH <sub>2</sub> | C   | C                                | a    | b                    | Ar1   | Ar2  | Ar3             | Ar4  | Ar5 | Ar6 | Ar1  | Ar2 | Ar3             | Ar4  | Ar5 | Ar6  | ArOCH <sub>2</sub> | CO   |     |     |
| NMR | 0.6      | -0.3            | -0.4 | -0.5            | 1.0 | 3.1                              | -4.2 | -3.3                 | -2.2  | -3.1 | 4.5             | 4.5  | 3.3 | 1.0 | 5.1  | 7.1 | -19.9           | 2.2  | 1.2 | 5.2  | 0.8                | -0.2 | 7.4 | 9.1 |
| DFT | 0.8      | -1.2            | -1.3 | 0.1             | 1.6 | 2.2                              | -4.2 | -1.6                 | -10.0 | -5.4 | 5.8             | 12.8 | 3.3 | 2.7 | -0.3 | 8.6 | -11.4           | -1.6 | 2.7 | 10.8 | 2.4                | -3.1 | 0.4 | 9.1 |

\* $\Delta\delta$  (ppm) =  $\delta$  ( $\text{Pb}^{2+}\text{-C}$  **1**) -  $\delta$  (**0**).

In the case of the carbon-13 chemical shifts, the largest differences are recorded for the carbonyl, OCH<sub>2</sub>CO and CH<sub>2</sub>OCH<sub>2</sub> carbon atoms, which move downfield, and for the aromatic carbon atom Ar1 (see Figure 5c) and the ArCH<sub>2</sub>Ar bridge carbon atoms, which move upfield (Table 2, Figure 6). A more pronounced effect is observed on ring B resonances upon  $\text{Pb}^{2+}$  binding, compared to those of ring A, mainly for the aromatic carbon atom 1 (-19.9 ppm and -2.2 ppm, respectively). The deshielding effect observed for the carbon atoms of OCH<sub>2</sub>CO groups indicates the involvement of the phenoxy and carbonyl oxygen atoms in complexation. In addition, the deshielding observed for the CH<sub>2</sub>OCH<sub>2</sub> carbon atoms, although smaller, may also indicate some interaction of the oxygen bridge with  $\text{Pb}^{2+}$  cation. The  $^{13}\text{C}$  NMR data seem to confirm a complexation mode where the cation is binding through the four carbonyl and the four phenoxy oxygen atoms.

With regard to the hexahomotrioxa ketone **2**, its cone conformation with  $C_{3v}$ -symmetry is reflected by its  $^1\text{H}$  and  $^{13}\text{C}$  NMR spectra. The former spectrum shows one AB quartet for the CH<sub>2</sub> bridge protons, and one singlet for the *tert*-butyl, aromatic and methylene protons of the OCH<sub>2</sub>CO groups. In addition, a series of multiplets for the adamantyl groups is also present. The latter spectrum exhibits a pattern containing five downfield resonances arising from the carbonyl and aromatic carbon atoms, two midfield resonances arising from the methylene carbon atoms of the OCH<sub>2</sub>CO and CH<sub>2</sub>OCH<sub>2</sub> groups, and six upfield resonances arising from the adamantyl and *tert*-butyl groups. As observed before for ketone **1**, the addition of  $\text{Pb}^{2+}$  cation affects all the proton and carbon-13 chemical shifts in ligand **2** (Table S3). The largest variations are recorded for the aromatic protons and the methylene protons of the OCH<sub>2</sub>CO groups, which move downfield, and by the oxygen bridge equatorial methylene protons, which move upfield. The  $\Delta\delta_{\text{Hax-Heq}}$  increases from 0.26 ppm to 0.52 ppm upon  $\text{Pb}^{2+}$  complexation. If Gutsche criterion is also applicable to the CH<sub>2</sub>OCH<sub>2</sub> bridges, it indicates that the phenyl groups in ketone **2** are more flattened than those in ketone **1**, and stand up when the cation enters into the binding cavity, resulting in a more regular cone conformation. Concerning  $^{13}\text{C}$  chemical shifts, the largest downfield differences are observed for the carbonyl and OCH<sub>2</sub>CO carbon atoms, while an upfield shift is observed for the aromatic carbon atom 1 (Table 3, Figure 7). The spectroscopic data indicate a similar binding mode to the one observed before for ketone **1**, with  $\text{Pb}^{2+}$  bound through metal-oxygen interactions inside the ionophoric cavity.

**Table 3.**  $^{13}\text{C}$  NMR chemical shift variations\* for ligands **2** and **3** upon  $\text{Pb}^{2+}$  complexation obtained by NMR and DFT (M06-2X) calculations. See Figure 5c for atom identification.

|     | ketone 2 |                 |      |                 |     |                                  |                    |      |       |      |     |      |
|-----|----------|-----------------|------|-----------------|-----|----------------------------------|--------------------|------|-------|------|-----|------|
|     | t-Bu     |                 | Ad   |                 |     |                                  | Aromatic ring      |      |       |      |     |      |
|     | C        | CH <sub>3</sub> | CH   | CH <sub>2</sub> | C   | CH <sub>2</sub> OCH <sub>2</sub> | ArOCH <sub>2</sub> | CO   | Ar1   | Ar2  | Ar3 | Ar4  |
| NMR | 0.3      | -0.4            | -0.4 | -0.6            | 1.2 | 1.4                              | 4.3                | 7.9  | -3.6  | -0.3 | 4.0 | 4.5  |
| DFT | 0.7      | -1.2            | -1.7 | -1.0            | 3.4 | 1.2                              | -2.9               | 16.5 | -13.2 | -3.7 | 4.9 | 11.3 |
|     | ketone 3 |                 |      |                 |     |                                  |                    |      |       |      |     |      |
| NMR | -0.2     | -1.0            | -1.2 | -1.3            | 0.4 | -3.8                             | 6.8                | 7.0  | -6.0  | 0.1  | 0.7 | 4.1  |
| DFT | 0.1      | -1.3            | -1.4 | -1.0            | 2.2 | -4.9                             | 3.2                | 13.2 | -11.8 | -1.6 | 2.8 | 11.3 |

\* $\Delta\delta$  (ppm) =  $\delta$  ( $\text{Pb}^{2+}$  ligand) -  $\delta$  (ligand)

Finally, calix[4]arene ketone **3** also presents symmetric proton and carbon-13 NMR spectra, compatible with a cone conformation. Upon  $\text{Pb}^{2+}$  complexation, the largest downfield variations are recorded for the aromatic protons and the bridging equatorial methylene protons, while the highest upfield change is observed for the bridging axial methylene protons (Table S4). In this case, the  $\Delta\delta_{\text{Hax-Heq}}$  decreases from 1.72 ppm to 0.57 ppm being, among the three ligands, the closest value to 0.9 ppm, indicating that ketone **3** adopts a more symmetric cone conformation upon complexation. In the case of the  $^{13}\text{C}$  chemical shift variations upon complexation (Table S4), the highest values are recorded for both carbonyl and methylene carbon atoms of the  $\text{OCH}_2$  CO groups, which move downfield, and for the aromatic carbon atom Ar1, which moves upfield, being all similar in absolute value (Table 3, Figure 7). This suggests that  $\text{Pb}^{2+}$  cation should be centred inside the ionophoric cavity, interacting equally with the eight oxygen atoms.

The X-ray results have shown the inclusion of an acetonitrile molecule in the hydrophobic cavity of ligands **1** and **3**, and the impact on their conformations.

Thus, to see if the MeCN had also a role in the complexation process in solution, as described for calix[4]arene analogues [39,44], additional  $^1\text{H}$  NMR experiments were carried out. Free and complexed ligands **1** and **3** were titrated with MeCN in  $\text{CDCl}_3$ . No effects were observed for ligand **1** (free or complexed) and for free ligand **3** (Figure S3a). The chemical shift of the MeCN protons remained unchanged at 2.0 ppm during the titration (up to 7 equiv). In the case of  $\text{Pb}^{2+}$  ketone **3** complex (1:1), a small effect could be detected: the MeCN resonance appeared at 1.85 ppm in the beginning of the titration and slightly shifted to 1.91 ppm after the addition of 10 equiv of MeCN (Figure S3b). This corresponds to a small upfield shift ( $\Delta\delta = -0.25$  ppm) relative to its normal position in  $\text{CDCl}_3$  ( $\delta = 2.10$  ppm), and indicates some inclusion of this molecule in the hydrophobic cavity of ligand **3**. However, the proton signals of **3** remained almost unchanged throughout the titration. This result may indicate that, in this case, the affinity of the complex for MeCN is slightly higher than that of the free ligand, due to a better preorganisation of the hydrophobic cavity of the former.

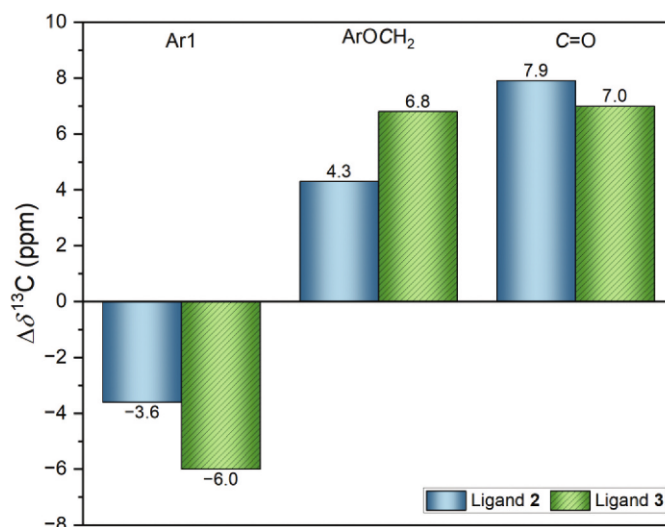


**Figure 7.** Largest  $^{13}\text{C}$  chemical shift differences for ligands **2** and **3** upon  $\text{Pb}^{2+}$  complexation [ $\delta$  ( $\text{Pb}^{2+}$  ligand) -  $\delta$  (ligand)].



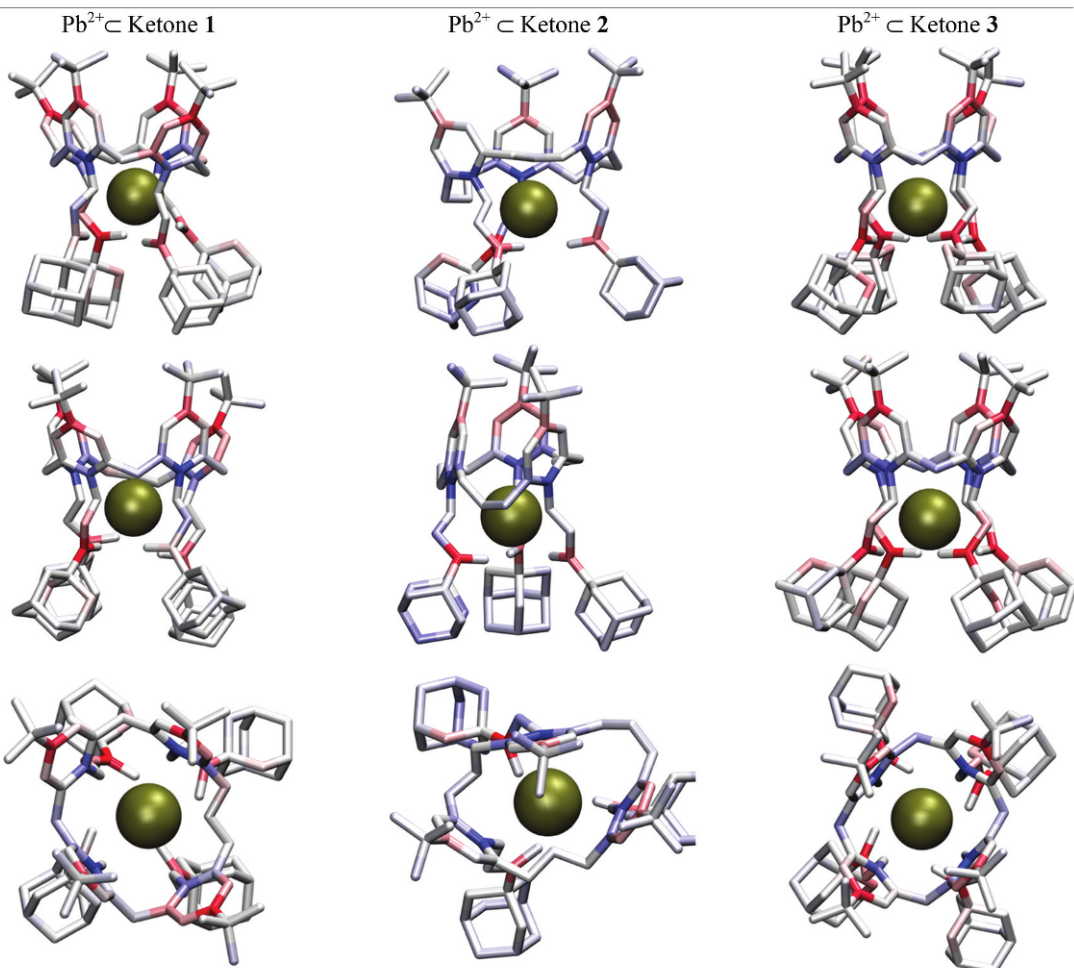


**Figure 8.** Structures of the  $\text{Pb}^{2+} \subset \text{ketone}$  complexes calculated at the M06-2X DFT level.  $^{13}\text{C}$  NMR chemical shift variations [ $\delta(\text{Pb}^{2+} \subset \text{ketone}) - \delta(\text{ketone})$ ], negative in blue and positive in red (front, orthogonal and top views).

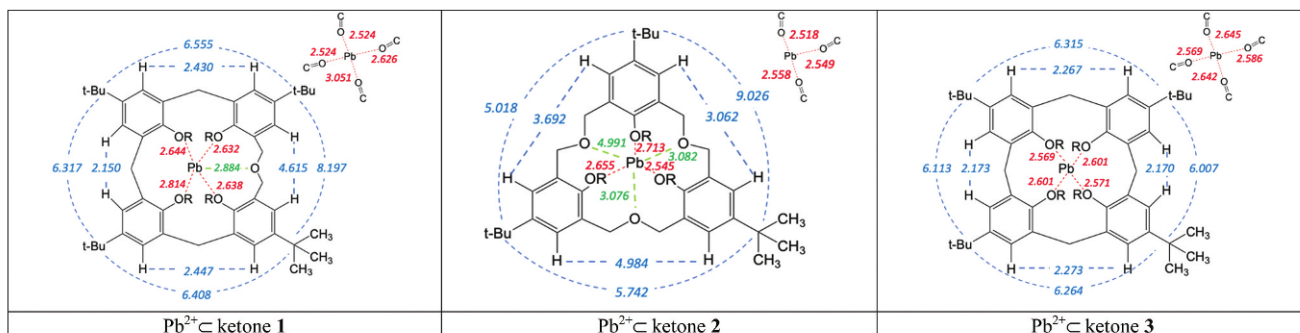


**Figure 9.** Relevant distances (in Å) in structures of the  $\text{Pb}^{2+} \subset \text{ketone}$  complexes calculated at the M06-2X DFT level; R =  $\text{CH}_2\text{COAD}$ .

To complement the previous studies, DFT optimisations of the  $\text{Pb}^{2+} \subset \text{ketone}$  complexes in the presence of an acetonitrile molecule in the hydrophobic cavity were performed. Overall, there are very little structural differences between the structures with and without acetonitrile (Figure S4). The RMSD fluctuations, for each ligand, between mono and di-complexed structures are 0.114. Lead coordination sphere remains unchanged despite

the presence of a solvent molecule sitting in the ligand hydrophobic cavity.

#### Quantum Mechanical calculations

Geometry optimisations were performed on free and complexed ligands with four different DFT functionals (B3LYP, BP86, M06-2X and wB97XD). The M06-2X functional was selected as in general it showed the best

**Table 4.** Relevant distances (in Å) for free ketones and their Pb<sup>2+</sup> complexes calculated at the M06-2X DFT level.

|   | ketone 1 | ketone 2 | ketone 3 | Pb <sup>2+</sup> ⊂ 1 | Pb <sup>2+</sup> ⊂ 2 | Pb <sup>2+</sup> ⊂ 3 |
|---|----------|----------|----------|----------------------|----------------------|----------------------|
| C <sub>t-Bu</sub> ⋯ C <sub>t-Bu</sub> in adjacent rings | 6.470    | 5.321    | 6.489    | 6.317                | 5.018                | 6.007                |
|   | 6.600    | 5.363    | 6.807    | 6.408                | 5.742                | 6.113                |
|   | 6.652    | 9.295    | 6.851    | 6.555                | 9.026                | 6.264                |
|   | 9.094    |          | 7.521    | 8.197                |                      | 6.315                |
| H <sub>arom</sub> ⋯ H <sub>arom</sub> in adjacent rings | 2.573    | 3.196    | 2.664    | 2.150                | 3.062                | 2.170                |
|   | 2.682    | 3.517    | 2.735    | 2.430                | 3.692                | 2.172                |
|   | 2.854    | 4.878    | 3.013    | 2.447                | 4.984                | 2.267                |
|   |          |          | 3.034    | 4.615                |                      | 2.273                |
|   | 5.073    |          |          |                      |                      |                      |

performance for the calculation of the <sup>13</sup>C NMR chemical shifts. Similar results with this functional and calix[4] arene derivatives have been reported [45]. A comparison between experimental and theoretical chemical shifts provides practical information on the chemical structure and conformation of the macrocycles and their complexes. The <sup>13</sup>C chemical shifts obtained with all functionals used are given in Tables S5-S7, and they are only slightly dependent on the functional, being in agreement with the experimental values (see Tables 2 and 3). In a few cases, variations larger than 2 ppm were observed.

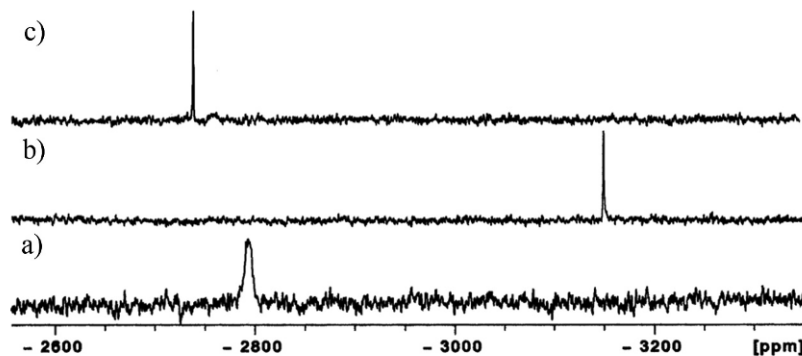
Independently from the chosen functional, the Δ*E* complexation energies [Δ*E* = *E* (complex) – *E* (free ligand) – *E* (Pb<sup>2+</sup>)] follow the same order for the three ligands: ketone **1** > ketone **3** > ketone **2**, thus being ketone **1** the best ligand for Pb<sup>2+</sup> cation (Table S8). The Δ*E* values obtained with M06-2X functional are –254.2, –237.4 and –225.6 kcal mol<sup>–1</sup> for ketones **1**, **3** and **2**, respectively, showing quite large differences in the complexation energies. Functionals without dispersion correction present little differentiation among the ligand energies, while in the case of functionals wB97XD and M06-2X, including already dispersion corrections to some degree, and for the B3LYP and BP86 functionals with the Grimme D3 correction, the differences are higher (Table S8). It should be noted that dispersion correction is important to obtain accurate NMR chemical

shifts, especially for systems presenting weak intra- or intermolecular contacts [46].

A structural analysis of the different complexes shows significant differences depending on the ligand. Snapshots of the optimised Pb<sup>2+</sup> complexes are given Figure 8 and Figures S5 to S7, and the most relevant distances, especially Pb<sup>2+</sup> ⋯ O ones, are given in Figure 9 and Table 4 and S9.

Free ketone **1** has an asymmetrical conformation due to the presence of the CH<sub>2</sub>OCH<sub>2</sub> bridge, showing three shorter (~6.57 Å) and one longer (~9.09 Å) *t*-Bu ⋯ *t*-Bu distances. This leads to a flattened cone conformation, with one short (5.337 Å) and one long (12.722 Å) *t*-Bu ⋯ *t*-Bu distances between two opposite aryl groups. The two closest aryl groups have an almost parallel orientation. Concerning free ketone **2**, it exhibits also an asymmetrical conformation, with two shorter (~5.34 Å) and one longer (9.30 Å) *t*-Bu ⋯ *t*-Bu distances, leading to a distorted cone conformation. Finally, ketone **3**, with a symmetrical structure, presents also a flattened cone conformation, with a short (5.324 Å) and a long (12.230 Å) *t*-Bu ⋯ *t*-Bu distances between two opposite aryl groups (see Figures S5 to S7).

The Pb<sup>2+</sup> complexation tightens the ligand upper rim, as shown by the shorter *t*-Bu ⋯ *t*-Bu and H<sub>arom</sub> ⋯ H<sub>arom</sub> distances in the complexes compared to those of the corresponding free ligands (Table 4). The complexed ligand **1** leads to an asymmetrical structure, with a flattened cone conformation. Pb<sup>2+</sup> cation is surrounded by nine oxygen

**Figure 10.** <sup>207</sup>Pb NMR spectra in CDCl<sub>3</sub>/CD<sub>3</sub>OD (10:1) of: a) Pb(ClO<sub>4</sub>)<sub>2</sub>, b) 1:1 Pb<sup>2+</sup>⊂ **1** complex and c) 1:1 Pb<sup>2+</sup>⊂ **3** complex.

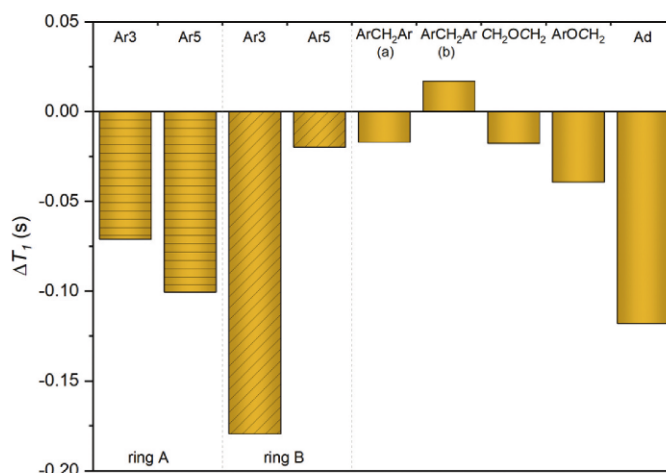


**Figure 11.** Relevant  $T_1$  variation for ligand **1** upon complexation [ $T_1(\text{Pb}^{2+} \subset \text{ligand } \mathbf{1}) - T_1(\text{ligand } \mathbf{1})$ ].

atoms, at a distance less than 3.05 Å: three of the four carbonyl oxygen atoms are the closest, at less than 2.6 Å, and the phenoxy oxygen atoms sit at about 2.6–2.9 Å (included the CH<sub>2</sub>OCH<sub>2</sub> one): This may explain the highest complexation energy obtained with ketone **1**. Ketone **3** shows a symmetrical structure, being the cation positioned in the centre of the cavity created by the four + four oxygen atoms of the pendant arms. All the Pb<sup>2+</sup>⋯oxygen distances are lower than 2.65 Å, which may also explain the higher interaction energy compared to ketone **2**, with only three pendant arms. The influence of the complexation on the ligand conformation is quite large in this case, changing ketone **3** from a flattened cone conformation to a square cone conformation upon complexation, as illustrated in Figure 8 and S7. Both *t*-Bu⋯*t*-Bu and H<sub>arom</sub>⋯H<sub>arom</sub> distances decrease, with variations up to 1.2 Å. The cone conformation of the complexed ligand **2** remains distorted and asymmetrical, although in the sphere of coordination around lead, composed by six oxygen atoms from the three pendant arms, the Pb<sup>2+</sup>⋯O distances are very similar and the shortest among the three studied complexes: around 2.5 Å for Pb<sup>2+</sup>⋯O<sub>C=O</sub> and from 2.5 to 2.7 Å for Pb<sup>2+</sup>⋯O<sub>phenoxy</sub>. The sphere of coordination is completed by two CH<sub>2</sub>OCH<sub>2</sub> bridge oxygens sitting at ~3.1 Å (Figure 9).

### <sup>207</sup>Pb NMR studies

The <sup>207</sup>Pb NMR experiments were performed to confirm the coordination environment of Pb<sup>2+</sup> cation in both ketones **1** and **3**, since the <sup>207</sup>Pb nucleus has a large chemical shift range (~17,000 ppm), being very sensitive to changes in its coordination sphere [47]. <sup>207</sup>Pb NMR studies with calix[4]arene-crowns-6 in acetonitrile have been reported [48]. Thus, <sup>207</sup>Pb spectra were obtained after the addition of the ligands to a CDCl<sub>3</sub>/CD<sub>3</sub>OD (10:1) solution of Pb(ClO<sub>4</sub>)<sub>2</sub>.

The <sup>207</sup>Pb NMR resonances of the complexed ketones **1** and **3** display sharp peaks at -3148.8 and -2738.8 ppm, respectively (Figure 10). This result shows that oxygen donor atoms produced large shielding effects in <sup>207</sup>Pb resonances and that the coordination number of Pb<sup>2+</sup> ion should be the same, in agreement with DFT results for both complexes. However, the presence of the CH<sub>2</sub>OCH<sub>2</sub> oxygen bridge in ketone **1**, an additional although weaker coordination site, may account for the further shielding effect observed in this case.

### Proton relaxation studies

The proton spin-lattice relaxation times ( $T_1$ ) of the free and complexed calixarenes were also determined to access the conformational changes of the ligands **1**, **2** and **3** upon Pb<sup>2+</sup> ion complexation. The  $T_1$  relaxation is mainly due to intramolecular dipolar interactions between the protons of the receptor in the free and bound species.

An analysis of the data (Tables S10-S12) shows a general decrease of  $T_1$  upon complexation in agreement with the increase of the molecular weight of the complexes. For the three ligands, at the upper rim level, the decrease is more pronounced for the aromatic protons than for the -CH<sub>2</sub>-bridge protons, as consequence of the conformational changes that decrease the average distances between adjacent aromatic protons in the Pb<sup>2+</sup> ⊂ ketone complexes (Figure 11, S8 and S9). This effect is confirmed by the average distances taken from the DFT optimised structures (Table S9), as for example 3.30/2.91 Å and 2.86/2.22 Å for ketones **1** and **3** and their Pb<sup>2+</sup> complexes, respectively. It was also observed that in case of ketone **2** the  $T_1$  values of the aromatic protons are not so sensitive to conformational changes upon complexation as they are in the case of ligands **1** and **3**, probably because in **2** the average distances are longer, 3.86/3.91 Å for **2** and its Pb<sup>2+</sup> complex, respectively. In the macrocycle lower rim, there is also

a significant decrease in the  $T_1$  average values of the adamantyl groups of ketones **1** and **3** upon complexation that may be related with the loss of mobility of the pendant arms upon  $Pb^{2+}$  coordination by both the phenoxy and the carbonyl oxygen atoms.

## Conclusions

The conformational changes of adamantyl ketones **1**, **2** and **3** upon  $Pb^{2+}$  complexation were established by NMR measurements in chloroform. The conformations of these 1:1 complexes deduced from  $^1H$  and  $^{13}C$  NMR experiments showed that  $Pb^{2+}$  ion is encapsulated in the cavity composed of the phenoxy and carbonyl oxygen atoms. In the case of dihomooxa ligand **1**, the data indicate a more flattened cone conformation upon complexation, with also some interaction of the  $CH_2OCH_2$  oxygen bridge with the cation. For the hexahomotrioxa ligand **2**, the phenyl groups seem more flattened compared to those of ligand **1**, and stand up after ion binding, resulting in a more regular cone conformation. Finally, calix[4]arene ligand **3** presents the more symmetric cone conformation upon complexation, with  $Pb^{2+}$  centred inside the ionophoric cavity and interacting equally with the eight oxygen atoms. The inclusion of a MeCN molecule in the hydrophobic cavity of the free and complexed ligands was also investigated by  $^1H$  NMR, but only in the case of  $Pb^{2+}$   $\subset$  ketone **3** complex such evidence was observed. These binding modes were, in general, corroborated by the DFT calculations. A good agreement was also obtained between DFT predicted and experimental  $^{13}C$  chemical shifts. The  $\Delta E$  complexation energies indicated that ketone **1** is the best  $Pb^{2+}$  ligand, apart from the functional used. The  $^{207}Pb$  NMR experiments further support the proposed  $Pb^{2+}$  coordination mode, and a general decrease of  $T_1$  values upon complexation is in agreement with the conformational changes observed for the three ligands.

The X-ray diffraction of the two pseudo-polymorphic crystals for both **1** and **3** derivatives has confirmed the cone conformation and revealed an interesting role of the acetonitrile guest molecule, with consequences on the conformation of the adamantyl and carbonyl pendant groups. In particular, in the dihomooxa ketone **1** the guest molecule open the cup, while in the calix[4]arene ketone **3** the pinched cone conformation becomes more symmetric.

## Disclosure statement

No potential conflict of interest was reported by the author(s).

## Funding

This work has received funding from Fundação para a Ciência e a Tecnologia, Project ref. UIDB/00100/2020, and infrastructure Project ref. 022161 (co-financed by FEDER through COMPETE 2020, POCI, PORL and FCT through PIDDAC).

## Reference

- [1] Toth G, Hermann T, Da Silva MR, et al. Heavy metals in agricultural soils of the European union with implication for food safety. *Environ Int.* **2016**;88:299–309.
- [2] Cicero CE, Mostile G, Vasta R, et al. Metals and neurodegenerative diseases. A systematic review. *Environ Res.* **2017**;159:82–94.
- [3] Reuben A. Childhood lead exposure and adult neurodegenerative disease. *J Alzheimer's Disease.* **2018**;64(1):17–42.
- [4] Gutsche CD. *Calixarenes*; monographs in supramolecular chemistry. Cambridge, UK: The Royal Society of Chemistry; 1989; Gutsche, C.D. *Calixarenes, An Introduction; Monographs in Supramolecular Chemistry; The Royal Society of Chemistry: Cambridge, UK, 2008.*
- [5] Neri P, Sessler JL, Wang M-X, Eds. *Calixarenes and beyond.* Switzerland: Springer International Publishing; 2016.
- [6] Deska M, Sliwa, W DB. Selected applications of calixarene derivatives. *ARKIVOC.* **2015**;2015(vi):393–416.
- [7] Espanol ES, Maldonado M. Host-guest recognition of pesticides by calixarenes. *Critical Rev Anal Chem.* **2019**;49(5):383–394.
- [8] Razuvayeva Y, Kashapov R, Zakharova L. Calixarene-based pure and mixed assemblies for biomedical applications. *Supramol Chem.* **2020**;32(3):178–206.
- [9] Arnaud-Neu F, McKervey MA, Schwing-Weill MJ. Metal-ion complexation by narrow rim carbonyl derivatives. In: Asfari Z, Böhmer V, Harrowfield J, et al., editors. *Calixarenes 2001.* Dordrecht: Kluwer Academic Publishers; 2001. p. 385–406.
- [10] Creaven BS, Donlon DF, McGinley J. Coordination chemistry of calix[4]arene derivatives with lower rim functionalisation and their applications. *Coord Chem Rev.* **2009**;253(7–8):893–962.
- [11] Kurniawan YS, Ryu M, Sathuluri RR, et al. Jumina. Separation of Pb(II) ion with tetraacetic acid derivative of calix[4]arene by using droplet-based microreactor system. *Indones J Chem.* **2019**;19(2):368–375.
- [12] Kurniawan YS, Sathuluri RR, Iwasaki W, et al. Jumina. microfluidic reactor for Pb(II) ion extraction and removal with an amide derivative of calix[4]arene supported by spectroscopic studies. *Microchem J.* **2018**;142:377–384.
- [13] Kocer MB, Erdogan ZO, Oguz M, et al. A calix[4]arene-tren modified electrode for determination of lead ions in aqueous solution. *Org Commun.* **2019**;12(3):160–168.
- [14] Kucukkolbasi S, Sayin S, Yilmaz M. Fabrication and application of a new modified electrochemical sensor using

- newly synthesized calixarene-grafted MWCNTs for simultaneous determination of Cu(II) and Pb(II). *Acta Chim Slov.* **2019**;66:839–849.
- [15] Marcos PM. Functionalization and properties of homooxalixarenes. In: Neri P, Sessler JL, Wang M-X, editors. *Calixarenes and beyond*. Switzerland: Springer International Publishing; **2016**. p. 445–466.
- [16] Marcos PM, Félix S, Ascenso JR, et al. Complexation and transport of alkali and alkaline earth metal cations *p*-*tert*-butyldihomooxalix[4]arene tetraketone derivatives. *Supramol Chem.* **2006**;18(4):285–297.
- [17] Marcos PM, Félix S, Ascenso JR, et al. Complexation and transport of transition and heavy metal cations by *p*-*tert*-butyldihomooxalix[4]arene tetraketones and X-ray crystal structure of the *tert*-butyl ketone derivative. *New J Chem.* **2007**;31(12):2111–2119.
- [18] Marcos PM, Ascenso JR, Segurado MAP, et al. Synthesis, binding properties and theoretical studies of *p*-*tert*-butylhexahomotrioxalix[3]arene tri-(adamantyl)ketone with alkali, alkaline earth, transition, heavy metal and lanthanide cations. *Tetrahedron.* **2009**;65(2):496–503.
- [19] Fonseca JD, Marcos PM, Ascenso JR, et al. Extraction and complexation of lanthanide ions by dihomooxalix[4]arene and calix[4]arene tetraketone derivatives: an experimental and molecular dynamics investigation. *C R Chimie.* **2019**;22(9–10):639–647.
- [20] Félix S, Ascenso JR, Lamartine R, et al. Synthesis and conformational analysis of *p*-*tert*-butyldihomooxalix[4]arene derivatives containing the carbonyl group. *Tetrahedron.* **1999**;55(28):8539–8546.
- [21] Arnaud-Neu F, Collins EM, Deasy M, et al. X-ray crystal structures, and cation-binding properties of alkyl calixaryl esters and ketones, a new family of macrocyclic molecular receptors. *J Am Chem Soc.* **1989**;111(23):8681–8691.
- [22] Kabsch WXDS. *Acta Crystallogr. Sect D Biol Crystallogr.* **2010**;66(2):125–132.
- [23] Kabsch W. Integration, scaling, space-group assignment and post-refinement. *Acta Crystallogr Sect D Biol Crystallogr.* **2010**;66(2):133–144.
- [24] Sheldrick GMSHELXT. Integrated space-group and crystal-structure determination. *Acta Crystallogr.* **2015**;A71:3–8.
- [25] Sheldrick GM. Crystal structure refinement with SHELXL. *Acta Crystallogr.* **2015**;C71:3–8.
- [26] Farrugia LJ, Win GX. WinGX and ORTEP for windows : an update. *J Appl Crystallogr.* **2012**;45(4):849–854.
- [27] Vold RL, Waugh JS, Klein MP, et al. Measurement of spin relaxation in complex systems. *J Chem Phys.* **1968**;48(8):3831–3832.
- [28] Frisch MJ, Trucks GW, Schlegel HB, et al. *Gaussian 16 Rev. B.01*. Wallingford, CT. p. 2016.
- [29] Becke AD. Density-functional thermochemistry. III. The role of exact exchange. *J Chem Phys.* **1993**;98(7):5648–5652.
- [30] Becke AD. Density-functional exchange-energy approximation with correct asymptotic behavior. *Phys Rev A.* **1988**;38(6):3098–3100.
- [31] Zhao Y, Truhlar DG. The M06 suite of density functionals for main group thermochemistry, thermochemical kinetics, noncovalent interactions, excited states, and transition elements: two new functionals and systematic testing of four M06-class functionals and 12 other functionals. *Theory Chem Acc.* **2008**;120:215–241.
- [32] Chai J-D, Head-Gordon M. Long-range corrected hybrid density functionals with damped atom–atom dispersion corrections. *Phys Chem Chem Phys.* **2008**;10(44):6615–6620.
- [33] Grimme S, Antony J, Ehrlich S, et al. A consistent and accurate ab initio parametrization of density functional dispersion correction (DFT-D) for the 94 elements H–Pu. *J Chem Phys.* **2010**;132(15):154104–154119.
- [34] Wolinski K, Hinton JF, Pulay P. Efficient implementation of the gauge-independent atomic orbital method for NMR chemical shift calculations. *J Am Chem Soc.* **1990**;112(23):8251–8260.
- [35] Bocheńska M, Cragg PJ, Guziński M, et al. Ion-selective electrodes based on *p*-*tert*-butyl-homooxalixarene di(ethyl)amides. *Supramol Chem.* **2009**;21(8):732–737.
- [36] Gattuso G, Notti A, Parisi MF, et al. Selective recognition of biogenic amine hydrochlorides by heteroditopic dihomooxalix[4]arenes. *New J Chem.* **2015**;39(2):817–821.
- [37] Teixeira FA, Marcos PM, Ascenso JR, et al. Selective binding of spherical and linear anions by tetraphenyl(thio)urea-Based dihomooxalix[4]arene receptors. *J Org Chem.* **2017**;82(21):11383–11390.
- [38] Noruzi EB, Shaabani B, Geremia S, et al. Biological activity of a multidentate calix[4]arene ligand doubly functionalized by 2-hydroxybenzeledene-thiosemicarbazone. *Molecules.* **2020**;25(2):370.
- [39] Danil de Namor AF, Chahine S, Kowalska D, et al. Selective interaction of lower rim calix[4]arene derivatives and bivalent cations in solution. Crystallographic evidence of the versatile behaviour of acetonitrile in lead(II) and cadmium(II) complexes. *J Am Chem Soc.* **2002**;124:12824–12836.
- [40] Beer PD, Drew MGB, Leeson PB, et al. Versatile cation complexation by a calix[4]arene tetraamide (L). Synthesis and crystal structure of [ML][ClO<sub>4</sub>]<sub>2</sub>·nMeCN (M = Fe<sup>II</sup>, Ni<sup>II</sup>, Cu<sup>II</sup>, Zn<sup>II</sup> or Pb<sup>II</sup>). *J Chem Soc Dalton Trans.* **1995**;8:1273–1283. DOI:10.1039/DT9950001273
- [41] Fonseca JD Síntese e aplicações de calixarenos na complexação de cátions com interesse ambiental. Report of *projecto tecnológico I*, FCUL, **2009**.
- [42] Marcos PM, Ascenso JR, Lamartine R, et al. NMR conformational studies of tetraalkylated dihomooxalix[4]arenes. *Tetrahedron.* **1997**;53:11791–11802.
- [43] Jaime C, de Mendoza J, Prados P, et al. Carbon-13 NMR chemical shifts. A single rule to determine the conformation of calix[4]arenes. *J Org Chem.* **1991**;56(10):3372–3376.
- [44] Horvat G, Stilinovic V, Hrenar T, et al. An integrated approach (thermodynamic, structural, and computational) to the study of complexation of alkali-metal cations by a lower-rim calix[4]arene amide derivative in acetonitrile. *Inorg Chem.* **2012**;51(11):6264–6278.
- [45] Guzzo RN, Rezende MJC, Kartnaller V, et al. Experimental and DFT evaluation of the <sup>1</sup>H and

- <sup>13</sup>C NMR chemical shifts for calix[4]arenes. *J Mol Struc.* **2018**;1157:97–105.
- [46] Beran GJO. Calculating nuclear magnetic resonance chemical shifts from density functional theory: a primer. *eMagRes.* **2019**;8:215–226.
- [47] Wrackmeyer B, Horchler K, Webb GA. <sup>207</sup>Pb-NMR Parameters. In: Webb GA, editor. Annual report on NMR spectroscopy. Vol. 22. San Diego, CA: Academic Press; **1990**. p. 249–306.
- [48] Bauer D, Blumberg M, Köckerling M, et al. A comparative evaluation of calix[4]arene-1,3--crown-6 as a ligand for selected divalent cations of radiopharmaceutical interest. *RSC Adv.* **2019**;9 (55):32357–32366.